Self-assembled dithiothreitol on Au surfaces for biological applications: phospholipid bilayer formation

Tânia B. Creczynski-Pasa,[a] M. Antonieta Daza Millone,[b] Maximiliano L. Munford,[c] Vânia R. de Lima,[a] Tiago O. Vieira,[a] Guillermo A. Benitez,[b] André A. Pasa,*[a] Roberto C. Salvarezza[b] and María E. Vela*[b]

Received 17th July 2008, Accepted 5th November 2008
First published as an Advance Article on the web 24th December 2008
DOI: 10.1039/b811964c

Self-assembly of dithiothreitol (DTT) on Au(111) from solution deposition has been studied by X-ray photoelectron spectroscopy and electrochemical data. DTT molecules self-assemble on Au(111) in a lying-down configuration irrespective of the concentration and temperature. XPS and electrochemical data indicate a DTT surface coverage of $\theta \approx 0.16$ with two S-head–Au covalent bonds per DTT molecule. The DTT monolayer turns the Au surface hydrophilic enough to allow the formation of fluid dimyristoylphosphatidylcholine (DMPC) bilayer domains by vesicle fusion as revealed by *in situ* atomic force imaging. Methylene blue (MB) and flavin adenine dinucleotide (FAD) have been used as probes to study molecule transport across the bilayer.

1. Introduction

Lipid membranes of living cells are the most important barriers to control the majority of cellular processes. They play a fundamental role in cell-to-cell communication involving the exchange of ions and biomolecules, including calcium, neurotransmitters, proteins, reactive species, and drugs among others.

Phospholipid bilayers can be taken as a model system of cell membranes because they preserve 2-D fluidity and can be modified with membrane proteins, ion channels, receptors and transporters, and can be used for various biotechnological applications.[1–3] Liposomes, in which phospholipid composition, structure and dynamics can be fully controlled, are generally accepted as a suitable model for *in vitro* studies of cell membrane structures and properties.[4–6] Liposomes are vesicles formed by a lipidic bilayer, structurally similar to the lipidic matrix of a cell membrane. However, to perform studies with atomic force microscopy (AFM), a technique that allows the determination of morphological and mechanical properties of structures, the immobilization of the lipidic bilayer on a solid surface[7–10] is required. There exist several methods to spread phospholipids on a solid substrate in order to achieve a supported bilayer.[11] Among the most widely used methods are sequential transfer of two monolayers from the air–water interface *via* Langmuir–Blodgett (LB) and Langmuir–Schaefer (LS) techniques,[12,13] single bilayer spreading[14] and vesicle fusion.[15]

Lipidic membranes supported on inorganic material surfaces, *e.g.* gold and mica, yield important results related to phase transition, stability and morphology of the layers and are promising structures for the development of biosensors.[16–18] On these surfaces, however, the physical–chemical properties of the lipidic layers are significantly different from membranes in fluid environments.[19] A promising approach is to use self-assembled monolayers (SAMs) of thiol molecules on gold, since they can act as a bridge or a spacer between the inorganic surface and the assembled macromolecules. Modification of solid surfaces with a spacer to link phospholipids bilayers provides a selective anchoring layer to accommodate hydrophilic domains of proteins and enables the charge transport from one side of the membrane to the other side.[4–6,20]

Concerning the inorganic surface there is a particular interest in metallic substrates because they can be used as electrodes in electrochemical-based biosensors. Gold substrates are particularly attractive because they are biocompatible and inert materials that can be modified by simple solution chemistry without significant contamination.

Several approaches have been developed to support phospholipid bilayers on gold. Hybrid bilayers of phospholipids on alkanethiol[21] or thiophospholipid[22] SAMs on gold lead to well ordered and blocking artificial membranes but they lack a proper fluidity to resemble a biomimetic system. Adding a long thiolated linker to the phospholipid tethered bilayers[5,6] or performing vesicle fusion over long ($C_n > 11$) hydroxyl-terminated thiols[20,23] (as a hydrophilic surface is required for this strategy) improve fluid properties. However an increase in the length of the linker chain should hinder electron transfer.[24] Therefore the use of a very short spacer that turns the gold surface hydrophilic enough for vesicle fusion and allows an easy electron transfer should be a suitable choice to build an electrochemical biosensor. Unfortunately, short hydroxyalkanethiol SAMs, *e.g.* 2-mercaptoethanol, have a lower stability against reductive desorption[25] which greatly decrease the range of electrochemical sensing ability.

[a] *Departamento de Ciências Farmacêuticas and Departamento de Física, UFSC, C. P. 476, Florianópolis, 88.040-900, Brazil. E-mail: pasa@fisica.ufsc.br; Fax: +55 48 3234 0599*
[b] *INIFTA, CONICET-UNLP, La Plata, CC 16 Suc. 4, Argentina. E-mail: mevela@inifta.unlp.edu.ar; Fax: +54 221 425 4642*
[c] *Departamento de Física, UFV, Viçosa, Brazil*

According to the previously mentioned requirements, dithiothreitol (DTT) appears to be a good candidate for these purposes. In fact, it is a short α,ω-alkanedithiol with two hydroxyl groups that, if the molecule adopts a lying-down configuration, should be exposed to the environment (Fig. 1). DTT SAMs have been used to bind Ag^+ cations,[26] to immobilize gold nanoparticles,[27] to study heterogeneous binding of divalent metals,[28] and also to provide an hydroxylated substrate for sol–gel synthesis.[29] It has been reported that DTT self-assembly on Au(111) changes the contact angles of a water droplet on gold from 50° to 38°.[30,31] Also, a related molecule, cyclo-DTT enabled the formation of an hierarchical self-assembly of proteins to a gold surface *via* the disulfide moiety and opening the S–S bond.[32]

In this work, we have used DTT as a sulfur bridge to separate the lipidic membranes from the gold surface. DTT self-assembled monolayers on Au(111) were characterized by its electrodesorption curves. Results from scanning tunneling microscopy (STM) show that DTT molecules induce the formation of the typical monoatomic deep pits.[33] From X-ray photoelectron spectroscopy (XPS) data we can conclude that DTT molecules self-assemble in a lying down configuration. The OH-rich surface facilitates the formation of fluid dimyristoylphosphatidylcholine (DMPC) bilayer domains obtained by vesicle fusion as observed by *in situ* atomic force measurements (AFM). Electrochemical results using two molecular probes, methylene blue (MB) and flavin adenine dinucleotide (FAD), confirm that a continuous and fluid bilayer is formed on the DTT–Au surface.

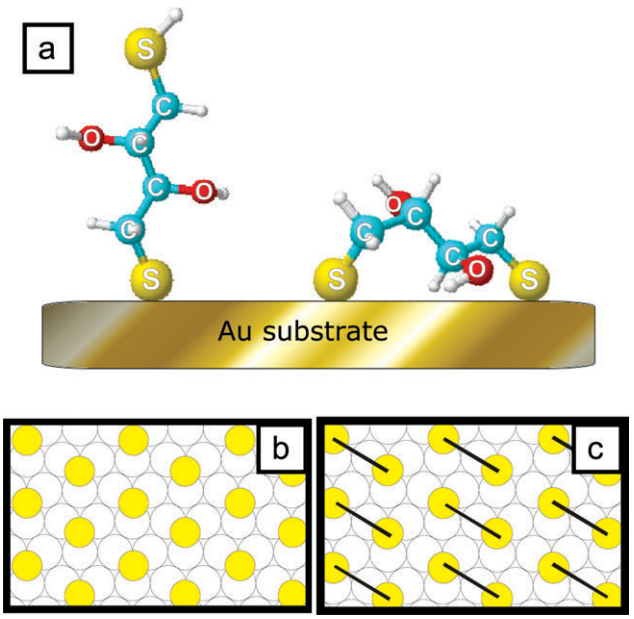

Fig. 1 (a) Representation of the DTT molecule according to a calculation using a PM3 semiempirical method. Each atom is labeled except hydrogens (white spheres). Standing up (left) and lying down (right) conformations. (b) $\sqrt{3} \times \sqrt{3}$ R30° structure for S heads (top circles) in the standing up configuration on the Au(111) substrate (white circles). (c) Lying down configuration of the bidentate molecules with S heads in a $\sqrt{3} \times \sqrt{3}$ R30° lattice.

2. Experimental

2.1 Substrates

Two different types of Au substrates were used. The first one was 250 nm thick gold films prepared by physical vapor deposition on a 4 nm chromium layer on glass (Gold Arrandee™). A three minute flame annealing was performed to generate a substrate consisting of atomically flat Au(111) terraces (Fig. 2a), separated by monoatomic steps. In these flat terraces atomic resolution of the Au(111) surface can be reached (Fig. 2b and inset). However, the root mean square roughness (rms) measured over 10 μm × 10 μm images is ≈12 nm due to the presence of deep grain boundaries between the atomically smooth large crystals. These substrates were used to study the self-assembly of DTT and to compare these results with those obtained for butanethiol monolayers. After DTT adsorption the typical monoatomic and diatomic deep pits formed during thiol self-assembly are observed (Fig. 2c, arrows).

The second type of substrates were thin films of vapor-deposited Au on silicon. The film consists of small grains of 20 nm in average size (Fig. 2d). Typical root mean square roughness values measured on 10 μm × 10 μm images are ≈3 nm. This substrate was used to prepare the phospholipid bilayers due to its low surface roughness and the absence of deep grain boundaries.

2.2 Chemicals

DL-Dithiothreitol (DTT), 1-butanethiol, 4-(2-hydroxyethyl)-1-piperazineethanesulfonic acid (HEPES) and flavin adenine

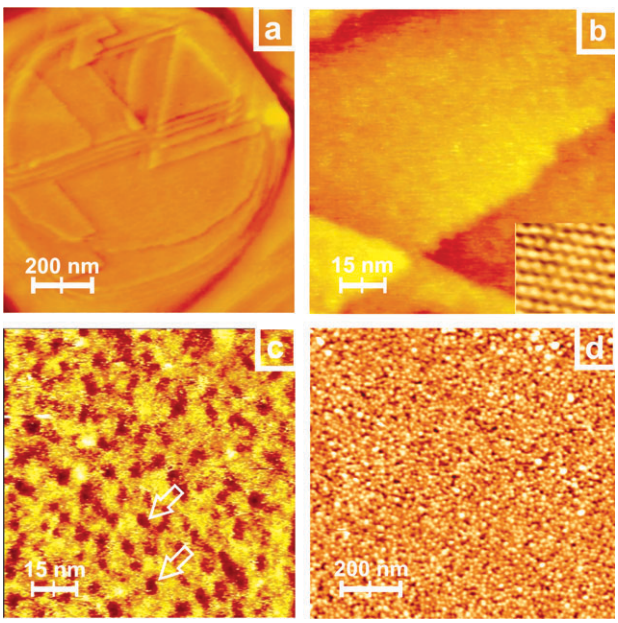

Fig. 2 (a) *Ex situ* 1 μm × 1 μm STM image of Au Arrandee™ substrate after H_2 flame annealing. (b) 75 nm × 75 nm STM image of smooth Au (111) terraces where atomic resolution is observed (inset 1.7 nm × 1.7 nm). (c) *Ex situ* 75 nm × 75 nm STM image of Au Arrandee™ substrate after incubation in 50 μM DTT ethanolic solution during 30 min at 60 °C. Note the formation of the typical pits produced by DTT adsorption (arrows show a couple of them). (d) *Ex situ* 1 μm × 1 μm AFM image of gold evaporated on Si(100). The image shows that the sample consists of grains ~20 nm in size.

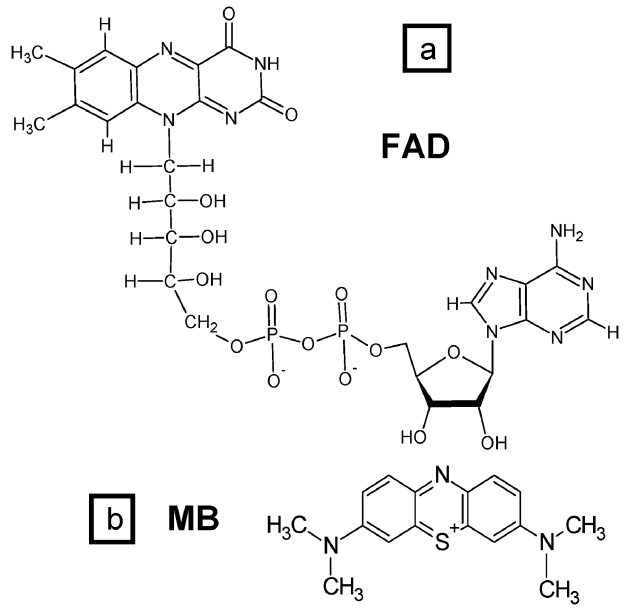

Fig. 3 (a) Flavin adenine dinucleotide and (b) methylene blue, both in their oxidized forms.

dinucleotide (FAD, Fig. 3a) were purchased from Sigma, dimyristoylphosphatidylcholine (DMPC) was purchased from Avanti and methylene blue (MB, Fig. 3b) from Merck. All other supplies used were of the best analytical grade commercially available.

2.3 Self-assembly and characterization of DTT SAMs

DTT SAMs were prepared by immersion of the gold substrates in 5 mM or 50 μM DTT ethanolic solution either at 25 °C or 60 °C for different times (t). Blank experiments using 50 μM butanethiol ethanolic solutions were also performed.

DTT SAMs were then analyzed by XPS, electrochemical measurements and *ex situ* STM. XPS measurements were performed using an Mg-Kα source (XR50, Specs GmbH) and a hemispherical electron energy analyzer (PHOIBOS 100, Specs GmbH). Spectra were acquired with 10 eV pass energy and a Shirley-type background was subtracted to each region. A two point calibration of the energy scale was performed using sputtered cleaned gold (Au 4f 7/2, binding energy = 84.00 eV) and copper (Cu 2p 3/2, binding energy = 933.67 eV) samples. C 1s at 285 eV was used as charging reference.

STM measurements were carried out with a Nanoscope IIIa (Veeco, Santa Barbara, USA). The presence of etched pits characteristic for chemisorption of thiols on gold are clearly visible (Fig. 2c). No molecular resolution was achieved under the experimental conditions used in this work.

Electrochemical measurements were performed in a conventional glass-made cell using the DTT-covered Au substrate as working electrode and a large Pt plate and a saturated calomel electrode as counter and reference electrodes, respectively, using a TEQ-2 potentiostat with data acquisition capability. Solutions were prepared with analytical-grade chemicals and Milli-Q water.

Reductive desorption measurements of DTT and butanethiol self-assembled monolayers were made following the procedure described elsewhere.[34,35] Briefly, a potential sweep was applied to the SAM-covered Au substrate immersed in a three-electrode electrochemical cell containing 0.1 M NaOH at 0.05 V s^{-1} from −0.4 V to −1.4 V.

Each solution was freshly prepared just before each series of measurements and deaerated with purified nitrogen.

2.4 Self-assembly of phospholipidic bilayers on DTT-covered Au substrates

DTT-covered Au prepared from 50 μM ethanolic solution at 60 °C for t = 30 min were used as substrates for supported bilayer formation by vesicle fusion.[30]

DMPC vesicles were obtained by evaporating, under a stream of nitrogen, the solvent of a phospholipidic solution (10 mg mL^{-1}) prepared in chloroform. The samples were dried under vacuum to eliminate solvent traces. Subsequently, multilamellar vesicles were obtained by the addition of a buffer containing 10 mM HEPES + 0.9% NaCl and vortexing. The multilamellar suspension was then extruded through a polycarbonate filter with 400 nm pore from Nuclepore to form unilamellar vesicles.[36,37]

DTT-covered Au substrates were immersed in 10 mg mL^{-1} DMPC unilamellar vesicle suspension for 90 min at ~30 °C (above DMPC phase transition temperature T_m = 23.9 °C) to allow vesicle fusion. The samples were then fast rinsed with 10 mM HEPES + 0.9% NaCl solution to remove the unbounded lipids, and immediately transferred to the AFM liquid cell. All AFM measurements were performed at pH 7.4 with a Molecular Imaging PicoScan microscope inside the fluid cell with temperature control, *i.e. in situ*, containing 10 mM HEPES + 0.9% NaCl, under contact mode with silicon nitride probes (triangular cantilevers with nominal spring constant of 0.12 N m^{-1}, Veeco Probes). The images were analyzed using the program VS × M 2.1 (Nanotec Electronica).

2.5 Electrochemical measurements with redox biomolecules

The experiments with the redox couples were performed in phosphate buffer 0.1 M pH = 7.0. The DTT–Au electrodes with or without the phosphilipidic bilayer were dipped in 0.1 mM methylene blue (MB) or 0.1 mM flavin adenine dinucleotide (FAD) aqueous solutions for 30 min at T = 37 °C. Potentials in the text are referred to the saturated calomel electrode (SCE).

3. Results and discussion

The self-assembly of DTT (DL-dithiothreitol) can be compared with the well-known self-assembly of short alkanethiolates. In principle, the DTT molecule can adopt two different configurations (standing up or lying down) on the Au(111) surface as schematically shown in Fig. 1a. Possible surface structures for those configurations considering the well-known surface structure reported for thiols,[33,38] dithiols[39–41] and DTT on Au(111)[30] are depicted in Fig. 1b and c.

Typical XPS data obtained for DTT-covered Au(111) surfaces prepared by immersion in 50 μM ethanolic solutions for t = 30 min at T = 60 °C are shown in Fig. 4a. After self-assembly, the sample was removed from the solution, carefully

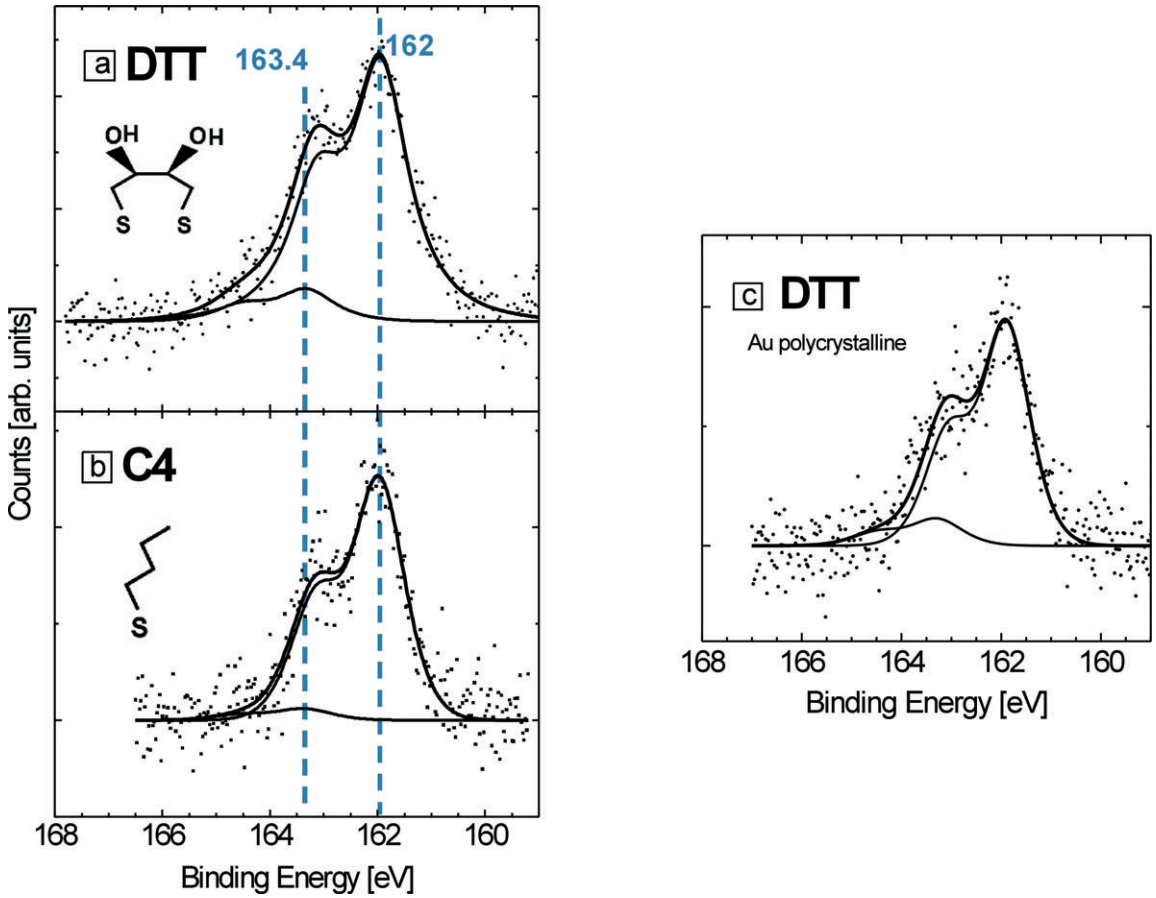

Fig. 4 XPS spectra (S 2p) taken from different thiol adlayers: (a) 30 min DTT 50 μM at 60 °C on Au(111), (b) 24 h butanethiol 50 μM at 25 °C on Au(111), (c) DTT on polycrystalline gold, incubated with the same conditions as for (a). Experimental points are represented by dots and the best fits by a continuous line. Main contributions are marked with dashed lines.

rinsed with ethanol and dried under a nitrogen flux before transferring to the UHV chamber. A broad XPS S 2p signal at 162–163 eV can be observed, a clear indication that thiols are present on the gold surface.[42] The S 2p signal was fitted by two doublets at 162 eV and 163.4 eV. The main component at 162 eV (Fig. 4a) corresponds to the S-head–Au covalent bonds as already reported[43] for different thiols on metal surfaces.[42] The smaller doublet at 163.4 eV corresponds to free SH groups which can be assigned either to physisorbed molecules that remain on the sample after the cleaning procedure or a small amount of molecules in standing up configuration (Fig. 1a).

Therefore, it can be concluded that the DTT molecules are chemisorbed mainly in a lying down configuration with two S-head–Au bonds per molecule (Fig. 1a, right). In fact, for DTT in the standing up configuration (Fig. 1a, left) we expect a significant contribution of the SH signal at 163.4 eV, which in this case is a minor contribution.

The S 2p (162 eV)/Au 4f signal ratio is a measure of the chemisorbed thiol coverage. We have used a self-assembled monolayer (SAM) formed on Au(111) by immersion in 50 μM butanethiol (C4) ethanolic solutions for $t = 24$ h (Fig. 4b) as reference system because, in this case, the SAM reaches its maximum surface coverage value $\theta \approx 0.33$, which corresponds to a $\sqrt{3} \times \sqrt{3}$ R30° surface structure of alkanethiol molecules in standing up configuration. Note that even in this case a small contribution of physisorbed thiol molecules at 163.4 eV is observed. In the C4 SAM (Fig. 4b) the S 2p (162 eV)/Au 4f signal ratio is ≈0.07. The spectrum shown in Fig. 4a for the DTT SAM also shows a S 2p/Au 4f signal ratio ≈0.07, which for a dithiol in the lying down configuration (Fig. 1, right) implies $\theta = 0.16$. Similar results were obtained using a higher concentration (5 mM) either at the same temperature ($T = 60$ °C) or lower ($T = 25$ °C) although for this concentration a greater contribution of the 163.4 eV component was observed. On the other hand, attempts to prepare the DTT SAM from 50 μM ethanolic solution at 25 °C for a self-assembly time of 30 min failed because we found a smaller S/Au ratio, *i.e.* the SAM does not completely cover the Au substrate. Based on the previous results we select 50 μM and 60 °C as the best experimental conditions to form a dense layer of lying down DTT molecules able to turn the Au highly hydrophilic.

In all cases the XPS spectra (Fig. 4) show no traces of oxidized S, such as sulfonates, since no signal was observed at 167–168 eV. Ageing of the sample in ambient condition leads to degradation of the DTT layer characterized by a strong S 2p signal at binding energies >167 eV. It is interesting to note that all DTT samples exhibit a clear O 1s signal contribution arising from the OH groups of the DTT molecules (data not shown).

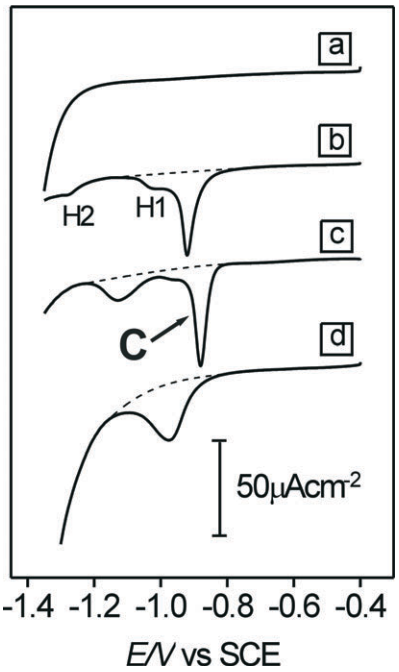

Fig. 5 *j vs. E* profiles for the reductive desorption of DTT and butanethiol SAMs. (a) Bare Au(111), (b) Au(111) incubated 30 min in DTT 50 μM at 60 °C, (c) Au (111) 24 h in butanethiol 50 μM at 25 °C and (d) polycrystalline gold 30 min in DTT 50 μM 60 °C. Measurements were made in NaOH 0.1 M at a sweep rate of 0.05 V s^{-1}.

We have obtained the same XPS results for DTT self-assembled on a vapor-deposited polycrystalline Au substrate (lying down configuration, $\theta = 0.16$) as can be seen in Fig. 4c. The self-assembly of a DTT monolayer on this surface is important for the preparation of continuous lipidic bilayers. As was mentioned in the Experimental section, polycrystalline Au (see Fig. 2d) exhibits a smooth surface consisting of nanometer-sized grains. On the other hand, preferred oriented Au(111) substrates have atomically smooth surface but they have deep grain boundaries that may produce discontinuities in the DMPC bilayer.

We have performed reductive electrodesorption curves to confirm the presence of the DTT covalently attached to the gold substrate. The electrolyte used in this case was NaOH 0.1 M because at neutral pH the current peak related to the thiol electrodesorption overlaps partially with the hydrogen evolution reaction (HER). The cathodic polarization curve shown in Fig. 5a corresponds to a clean (thiol SAM-free) preferentially oriented Au (111) substrate recorded from −0.4 to −1.4 V. Typical double layer response of gold, without any Faradaic current contributions, is observed preceding the large cathodic current related to HER. Fig. 5b shows typical curves recorded for DTT-SAM on the Au(111) prepared from the 50 μM ethanolic solutions for $t = 30$ min at $T = 60$ °C.

These polarization curves are compared with those obtained for butanethiol SAMs prepared by immersing the Au(111) substrate in 50 μM butanethiol ethanolic solution at 25 °C for 24 h (Fig. 5c). We have also included the polarization curve corresponding to a DTT SAM on polycrystalline Au prepared from 50 μM ethanolic solutions for $t = 30$ min at $T = 60$ °C (Fig. 5d).

In all cases, the current/potential profiles recorded for the thiol SAM-covered Au substrates show well defined cathodic current peaks followed by one or two humps preceding HER. As already reported the main cathodic current peak C corresponds to the reductive thiol desorption from the Au surface according to the reaction:[33]

$$1\bar{e} + \text{Au(111)–S–R} \rightarrow \text{R–S}^- + \text{Au(111)} \qquad (1)$$

Note that the current peak recorded for DTT electrodesorption from the polycrystalline Au is broader than those recorded in the preferred (111) oriented substrate due to the presence of different crystallographic faces, grain boundaries and large amount of defects.

First, we analyze the information related to the main peak C in Fig. 5. The peak potential (E_p) for DTT desorption from the Au(111) surface (Fig. 5b) is slightly negative in relation to that measured for a butanethiol (C4) SAM on the same substrate (Fig. 5c). Integration of the current involved in the electrodesorption peaks gives the charge density (q) corresponding to the amount of chemisorbed species. We have obtained a charge density of 73 ± 10 μC cm^{-2} which is consistent with S-head–Au bonds coverage ≈0.33 taking into account reaction (1) (one electron per chemisorbed sulfur atom) and a $\sqrt{3} \times \sqrt{3}$ R30° surface structure on the Au(111) surface. Note that this q value can be expected either for the DTT molecules chemisorbed in standing up ($\theta = 0.33$) or lying down ($\theta = 0.16$) configurations. Nevertheless, the standing up configuration is incompatible with XPS results (Fig. 4a).

Besides the main peak C, two humps H1 and H2 are observed at more negative potentials for DTT-SAM on Au(111). H1 is located on the negative side of the main desorption peak while H2 appears at −1.2 V. In contrast, only a small peak rather than a hump at −1.1 V is observed for butanethiol electrodesorption. This peak has been assigned to thiol molecules strongly chemisorbed at defects of the Au(111) surface such as steps.[44] Therefore, hump H2 can be assigned to DTT molecules adsorbed on Au defects. However, at present we have no clear interpretation on the origin of hump H1.

We have imaged the DTT SAM-covered Au samples by STM. Unlike butanethiol SAMs that exhibit the well-known $\sqrt{3} \times \sqrt{3}$ R30° and c(4 × 2) surface structures,[45] no molecular resolution could be achieved with DTT SAMs. As reported previously, this could be attributed to a more disordered layer.[30] However, DTT SAM formation can be inferred from the presence of the typical nanometer sized monoatomic and diatomic deep pits (Fig. 2c).

In principle, the lying down phase of DTT molecules (Fig. 1a, right) could provide a hydrophilic environment for anchoring different types of biomolecules. In the next paragraph we show that the DTT-SAMs can be used to form ordered phospholipidic bilayer domains on the polycrystalline Au surfaces. As mentioned above these substrates are particularly suitable for the formation of high quality bilayers due to its low roughness (Fig. 2d).

Fig. 6a–c shows *in situ* AFM images in buffer HEPES pH = 7.4 NaCl 0.9% of a vapor deposited polycrystalline Au covered by a DTT-SAM after immersion in a suspension of DMPC vesicles.

The surface morphology of the lipidic bilayer on DTT-SAM has the same characteristics (rms, grain size, *etc.*) as those exhibited by the clean polycrystalline Au substrate (Fig. 2d in Experimental section). As shown in Fig. 6a, large size areas (more than 10 μm × 10 μm) were *in situ* scanned with the AFM tip remaining stable during the time period of the experiments (≈4 h). In order to determine the presence of the lipidic layer we have used a lithographic step by applying an additional force to the cantilever probe. This procedure removes the material present in the scanned region opening a clear squared window, as displayed in Fig. 6b. This evidences that a soft material deposit covers the DTT–Au surface. In fact, complementary XPS data (not shown) of these samples reveal P, N and C, supporting the presence of a DMPC layer.

A line scan through the opened window region (Fig. 6b) provided a thickness of about 5 nm (Fig. 6d). Note that this value is slightly higher than the expected value for a DMPC bilayer (Fig. 7) due to the hydration of the DTT–DMPC interface.[8] It is interesting to note that on clean Au we were unable to form a lipidic layer since vesicles remained sphere-shaped on the surface. In consequence, a highly hydroxylated surface is needed for vesicle fusion necessary to form a bilayer film.

We have also been able to image the self-healing of this layer by lateral motion of phospholipids indicating that it is not rigid at 22 °C (Fig. 6c). The sequential AFM images allow a rough estimation of the lateral diffusion coefficient (D) of the phospholipids of the window (Fig. 6b and c). Taking a front displacement L for the time interval Δt and using $L^2 = 2D\Delta t$ we obtained $D \cong 10^{-11}$ cm^2 s^{-1}. This value is somewhat lower than that reported for DMPC bilayers supported on glass at this temperature (2×10^{-10} cm^2 s^{-1}).[46] The discrepancy can be explained either by a self-limiting spreading as discussed by Boxer[47] or by an increased interaction of DMPC with the underlying DTT/Au with respect to the glass substrate used by Smith *et al.*[46]

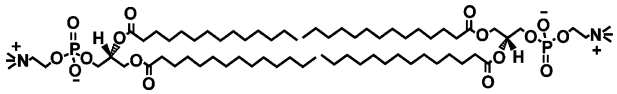

Fig. 7 Scheme showing two DMPC molecules linked by their lipidic tails.

The DMPC lateral motion points toward the maintenance of membrane dynamics, which is a signal that this system could be adequate for fundamental studies in general phenomena of natural membranes, such as the incorporation of biomolecules (enzyme cofactors, proteins, drugs, *etc.*).

Concerning this point, we have tested the behavior of our DMPC bilayer–DTT–Au arrangement when it was exposed to two electrochemically active molecules: methylene blue (MB), a lipophilic molecule able to penetrate biological membranes, and flavin adenine dinucleotide (FAD), an electron carrier, that is known to be unable to diffuse across the membrane.[48,49] The DMPC bilayer–DTT–Au substrates were immersed for 30 min in an aqueous solution containing MB or FAD at 37 °C in order to immobilize these molecules in the fluid bilayer. Afterwards, the substrates were removed from the solution, carefully rinsed with water to eliminate the MB and FAD molecules weakly bonded to the bilayer, and finally immersed in an electrochemical cell containing phosphate buffer at pH = 7.0 to detect the presence of the redox couples corresponding to immobilized molecules. The electrochemical response of the DMPC bilayer–DTT–Au substrates exposed to MB or FAD molecules was also compared to that exhibited for the bilayer-free DTT–Au substrates exposed to the same molecules under the same experimental conditions.

The voltammetric profiles (Fig. 8, dotted lines) show that the DTT–Au substrates have been able to immobilize certain amount of MB and FAD molecules since their redox couples are clearly observed.

On the other hand, for the DMPC bilayer–DTT–Au system only the redox couple of MB is electrochemically detected (Fig. 8, solid line) indicating that these molecules have been incorporated into the phospholipidic bilayer. The more irreversible electrochemical response of trapped MB into the bilayer demonstrates that they are placed at a larger distance from the DTT–Au substrate than in the absence of the bilayer. When FAD molecules are used as electrochemical probes, no electrochemical response is observed, *i.e.* they are not incorporated in the DMPC bilayer.

The electrochemical behavior of these molecular probes demonstrates the continuity and fluidity of our supported bilayers.

Bilayer continuity can be tested using the FAD probe. It is well established that FAD can not diffuse across membranes due to the presence of the pyrophosphate group[48] (Fig. 3a).

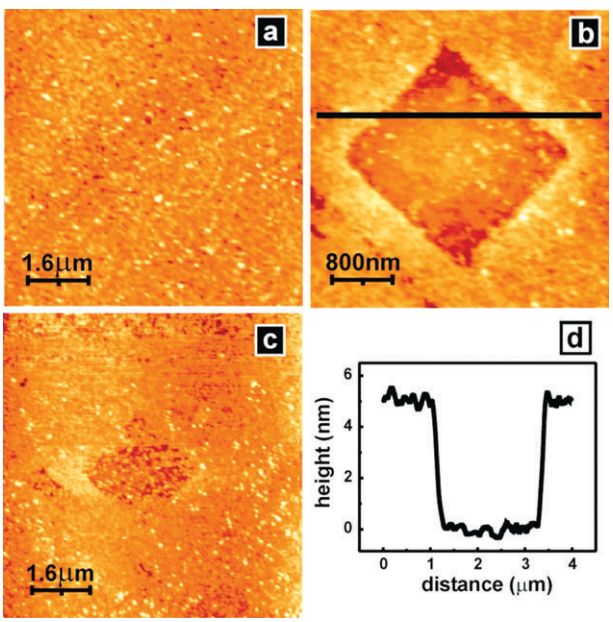

Fig. 6 AFM images of DMPC bilayer formed on a lying down DTT SAM formed on polycrystalline gold. (a) Large covered area with a lipid layer. (b) Square window defined by the removal of the lipid layer using the AFM tip. (c) DMPC layer recovering the surface of the square window, taken 120 s after image (b). (d) Cross section profile corresponding to the black line of image (b).

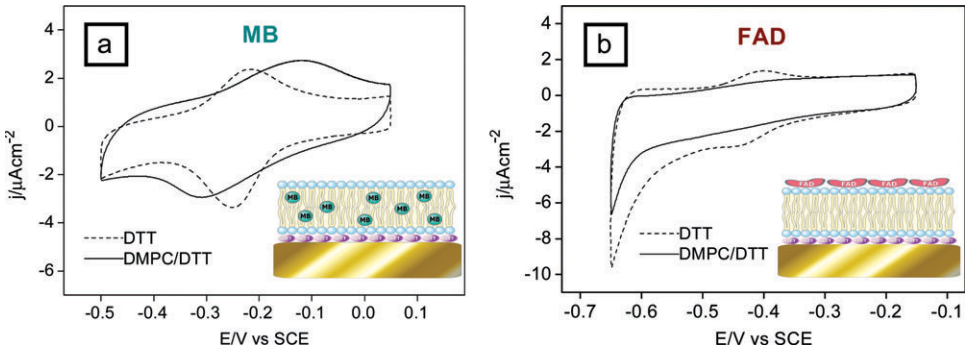

Fig. 8 Selective permeation of biomolecules. Cyclic voltammograms performed in phosphate buffer 0.1 M pH 7.0 at scan rate: 0.05 V s^{-1}. Full lines correspond to voltammograms for DMPC bilayer–DTT–Au (111) substrates incubated 30 min either in MB 0.1 mM (a) or FAD 0.1 mM (b) aqueous solutions to immobilize these molecules. Dotted lines correspond to the voltammograms recorded for DTT–Au(111) electrodes subjected to the same procedure.

FAD could only reach the DTT–Au interface and be electrochemically detected if significant defects like pores or discontinuities were present in the bilayer.

In addition to *in situ* AFM measurements, the MB probe permits fluidity testing. Diffusion of liposoluble molecules through rigid crystalline bilayers would be largely impeded.

4. Conclusions

* DTT molecules self-assemble on Au(111) mainly in a lying down configuration irrespective of the concentration and temperature. XPS and electrochemical data indicate a DTT surface coverage $\theta = 0.16$ with two S-head–Au covalent bonds per DTT molecule.

* The charge density involved in the electrodesorption curves for the DTT SAMs is the same that found for alkanethiols SAMs because the number of S-head–Au bonds remains constant.

* The peak potential for electrodesorption indicates that the stability of the DTT SAM is similar to that observed for butanethiolate SAM.

* DTT-SAMs on Au (111) are not highly ordered as no molecular resolution by STM was found during our STM imaging.

* DMPC bilayer membranes can be formed on DTT–Au because the surface is highly hydroxylated. The membranes exhibit self-healing behavior.

* The DMPC–DTT–Au system was used to test electrochemically the transport behavior of methylene blue and FAD across the bilayer, verifying that it is both fluid and continuous.

Acknowledgements

The authors wish to thank FAPESC, CAPES, CNPq/MCT, CONICET, ANPCyT (PICT 06-621, PAE 22771), for research grants and fellowships. V. R. de Lima is currently a PhD student of the Programa de Pós-Gradução em Química, UFSC. M. E. Vela is member of the research career of CIC BsAs.

References

1 Y. H. Chan and S. G. Boxer, *Curr. Opin. Chem. Biol.*, 2007, **11**, 581–587.
2 E. T. Castellana and P. S. Cremer, *Surf. Sci. Rep.*, 2006, **61**, 429–444.
3 R. P. Richter, R. Berat and A. R. Brisson, *Langmuir*, 2006, **22**, 3497–3505.
4 H. Lang, C. Duschl and H. Vogel, *Langmuir*, 1994, **10**, 197–210.
5 R. Naumann, A. Jonczyk, C. Hampel, H. Ringsdorf, W. Knoll, N. Bunjes and P. Gräber, *Bioelectrochemistry and Bioenergetics*, 1997, **42**, 241–247.
6 N. Bunjes, E. K. Schmidt, A. Jonczyk, F. Rippmann, D. Beyer, H. Ringsdorf, P. Gräber, W. Knoll and R. Naumann, *Langmuir*, 1997, **13**, 6188–6193.
7 J. Schneider, Y. F. Dufrene, W. R. Barger, Jr and G. U. Lee, *Biophys. J.*, 2000, **79**, 1107–1118.
8 F. Tokumasu, A. J. Jin and J. A. Dvorak, *J. Electron. Microsc. (Tokyo)*, 2002, **51**, 1–9.
9 T. Spangenberg, N. F. De Mello, T. B. Creczynski-Pasa, A. A. Pasa and H. Niehus, *Physica Status Solidi (A) Applied Research*, 2004, **201**, 857–860.
10 M. L. Munford, V. R. Lima, T. O. Vieira, G. Heinzelmann, T. B. Creczynski-Pasa and A. A. Pasa, *Microscopy and Microanalysis*, 2005, **11**, 90–93.
11 E. Sackmann and M. Tanaka, *Trends Biotechnol.*, 2000, **18**, 58–64.
12 L. K. Tamm and H. M. McConnell, *Biophys. J.*, 1985, **47**, 105–113.
13 A. Ulman, *An Introduction to Ultrathin Organic Films From Langmuir-Blodgett to Self-Assembly*, Academic Press, Inc., San Diego, 1991.
14 J. Raedler, H. Strey and E. Sackmann, *Langmuir*, 1995, **11**, 4539–4548.
15 A. A. Brian and H. M. McConnell, *Proc. Natl. Acad. Sci. USA*, 1984, **81**, 6159–6163.
16 P. K. W. Mary, L. Kraft, Marjorie L. Longo, Ian D. Hutcheon and Steven G. Boxer, *Science*, 2006, **313**, 1948–1951.
17 R. P. Richter and A. R. Brisson, *Biophys. J.*, 2005, **88**, 3422–3433.
18 S. Xu, G. Szymanski and J. Lipkowski, *J. Am. Chem. Soc.*, 2004, **126**, 12276–12277.
19 F. Tokumasu, A. J. Jin, G. W. Feigenson and J. A. Dvorak, *Biophys. J.*, 2003, **84**, 2609–2618.
20 W. Bücking, G. A. Urban and T. Nann, *Sensors and Actuators, B: Chemical*, 2005, **104**, 111–116.
21 A. L. Plant, M. Gueguetchkeri and W. Yap, *Biophys. J.*, 1994, **67**, 1126–1133.
22 M. B. Smith, J. Tong, J. Genzer, D. Fischer and P. K. Kilpatrick, *Langmuir*, 2006, **22**, 1919–1927.
23 M. Twardowski and R. G. Nuzzo, *Langmuir*, 2003, **19**, 9781–9791.
24 A. J. Bard and L. R. Faulkner, *Electrochemical methods: Fundamentals and Applications*, John Wiley & Sons, Inc., New York, 2001.
25 D. E. Weisshaar, M. M. Walczak and M. D. Porter, *Langmuir*, 1993, **9**, 323–329.
26 B. Zeng, X. Ding, D. Pan and F. Zhao, *Talanta*, 2003, **59**, 501–507.

27 L. Wang, J. Bai, P. Huang, H. Wang, L. Zhang and Y. Zhao, *Electrochem. Commun.*, 2006, **8**, 1035–1040.
28 D. Burshtain and D. Mandler, *Phys. Chem. Chem. Phys.*, 2006, **8**, 158–164.
29 J. T. Banks, T. T. Yu and H. Z. Yu, *J. Phys. Chem. B*, 2002, **106**, 3538–3542.
30 A. R. MacDairmid, M. C. Gallagher and J. T. Banks, *J. Phys. Chem. B*, 2003, **107**, 9789–9792.
31 R. G. Nuzzo and D. L. Allara, *J. Am. Chem. Soc.*, 1983, **105**, 4481–4483.
32 H. Wackerbarth, A. Pernille Tofteng, K. J. Jensen, I. Chorkendorff and J. Ulstrup, *Langmuir*, 2006, **22**, 6661–6667.
33 C. Vericat, M. E. Vela, G. A. Benitez, J. A. Martin Gago, X. Torrelles and R. C. Salvarezza, *J. Phys.: Condens. Matter*, 2006, **18**, R867–R900.
34 O. Azzaroni, M. E. Vela, G. Andreasen, P. Carro and R. C. Salvarezza, *J. Phys. Chem. B*, 2002, **106**, 12267–12273.
35 M. E. Vela, H. Martin, C. Vericat, G. Andreasen, A. Hernández Creus and R. C. Salvarezza, *J. Phys. Chem. B*, 2000, **104**, 11878–11882.
36 L. D. Mayer, M. J. Hope and P. R. Cullis, *Biochim. Biophys. Acta*, 1986, **858**, 161–168.
37 F. Olson, C. A. Hunt, F. C. Szoka, W. J. Vail and D. Papahadjopoulos, *Biochim Biophys Acta*, 1979, **557**, 9–23.
38 C. Love, L. A. Estroff, J. K. Kriebel, R. G. Nuzzo and G. M. Whitesides, *Chem. Rev.*, 2005, **105**, 1103–1169.
39 M. J. Esplandiu, M. L. Carot, F. P. Cometto, V. A. Macagno and E. M. Patrito, *Surface Science*, 2006, **600**, 155–172.
40 M. J. Esplandiu, H. Hagenström and D. M. Kolb, *Langmuir*, 2001, **17**, 828–838.
41 T. Y. B. Leung, M. C. Gerstenberg, D. J. Lavrich, G. Scoles, F. Schreiber and G. E. Poirier, *Langmuir*, 2000, **16**, 549–561.
42 D. G. Castner, K. Hinds and D. W. Grainger, *Langmuir*, 1996, **12**, 5083–5086.
43 C. Vericat, M. E. Vela, G. Andreasen, R. C. Salvarezza, L. Vázquez and J. A. Martín-Gago, *Langmuir*, 2001, **17**, 4919–4924.
44 C. Vericat, G. Andreasen, M. E. Vela, H. Martin and R. C. Salvarezza, *J. Chem. Phys.*, 2001, **115**, 6672–6678.
45 F. Terán Arce, M. E. Vela, R. C. Salvarezza and A. J. Arvia, *Langmuir*, 1998, **14**, 7203–7212.
46 B. A. Smith and H. M. McConnell, *Proc. Natl. Acad. Sci. USA*, 1978, **75**, 2759–2763.
47 S. G. Boxer, *Curr. Opin. Chem. Biol.*, 2000, **4**, 704–709.
48 M. Barile, C. Brizio, D. Valenti, C. De Virgilio and S. Passarella, *Eur. J. Biochem.*, 2000, **267**, 4888–4900.
49 F. Depeint, W. R. Bruce, N. Shangari, R. Mehta and P. J. O'Brien, *Chem. Biol. Interact.*, 2006, **163**, 94–112.

